

Optics Letters

Photoacoustic confocal dermoscope with a waterless coupling and impedance matching opto-sono probe

HAIGANG MA,¹ SIHUA YANG,^{1,2} ZHONGWEN CHENG,¹ AND DA XING^{1,3}

¹MOE Key Laboratory of Laser Life Science and Institute of Laser Life Science, College of Biophotonics, South China Normal University, Guangzhou 510631, China

²e-mail: yangsh@scnu.edu.cn

³e-mail: xingda@scnu.edu.cn

Received 3 April 2017; revised 19 May 2017; accepted 22 May 2017; posted 26 May 2017 (Doc. ID 291988); published 13 June 2017

Recently, intensive research on photoacoustic (PA) imaging has been conducted to accelerate the development of dermoscopy of the human skin. In this Letter, we first developed a PA dermoscope equipped with a waterless coupling and impedance matching opto-sono probe to achieve quantitative, high-resolution, and high-contrast imaging of the human skin. Compared with the commonly used liquid-coupled PA probes, the human-skin-adapted probe can facilitate implementation in the clinical setting. The non-invasive imaging experiments of epidermal and dermal structures in volunteers have been carried out to demonstrate the high imaging quality that can be obtained by using such an opto-sono probe for a PA dermoscope. The imaging results show the characteristic parameters of the skin, including pigment distribution and thickness, vascular diameter, and depth. The results confirm that the opto-sono probe can play an important role in the PA dermoscope for making clear the distribution of the pigment layer and blood vessels in the human skin. © 2017 Optical Society of America

OCIS codes: (170.0170) Medical optics and biotechnology; (170.5120) Photoacoustic imaging; (180.5810) Scanning microscopy; (170.3890) Medical optics instrumentation.

<https://doi.org/10.1364/OL.42.002342>

Skin photoacoustic (PA) microscopy is an emerging biomedical imaging that combines the high-contrast and spectroscopic-based specificity of optical imaging with the high spatial resolution of ultrasound imaging in a modality [1,2]. Scattering of ultrasonic in tissue is far less than the scattering of light; thus, PA microscopy can achieve images with high-resolution and high optical-absorption contrast extending into deep tissue and is superior to traditional dermoscopy [3–5]. In PA microscopes, the incident laser is usually focused into a spot laser, and then is used to illuminate biological tissues to generate ultrasonic signals. The detected ultrasonic signals are subsequently reconstructed into images; this process has come to be widely

applied in bio-medical imaging [6,7]. To enhance the sensitivity of PA microscopy, a focused ultrasound detector is commonly used to coaxially overlap the optical focus [8,9]. In order to assure the coaxial arrangement of laser illumination and ultrasound detection in PA microscopy systems, a hollow structured-focused detector is frequently adopted [10,11]. However, the acoustic lens/piezoelectric elements of focused detectors are mostly bowl structured [12,13], and usually utilize a sink or coupling cup to make the PA signal coupling in the ultrasonic detector. In the process, this approach can effectively reduce the reflective loss of PA signals, but the water is easy to pollute, needs to be replaced frequently, and forms fog or water droplets on the surface of the objective lens affecting the focusing effect directly, which will limit the human skin photoacoustic imaging and its clinical application [5,11]. In addition, the ultrasound detectors in most current medical imaging systems are made of piezoelectric composite or piezoelectric crystals [14,15]. Piezoelectric composite and piezoelectric crystals have an advantage of high electromechanical efficiency and stability and are suitable for manufacturing ultrasonic detectors, but the high acoustic impedance (the acoustic impedance of them is generally not less than 8 MRayl) makes it very difficult to implement acoustic matching with a human skin tissue (the acoustic impedance of human skin tissue is about 1.5 MRayl) [16,17]. Thus, in this Letter, we developed a waterless coupling and impedance matching opto-sono probe to effectively achieve high spatial resolution and sensitivity for a human PA dermoscope. The probe is mainly composed of an adjustable objective lens and an opto-sono detector. In addition, the detector is mainly composed of an opto-sono polystyrene (PS) lens and a hollow bowl polyvinylidene fluoride (PVDF) element. The PS lens has a high transmission efficiency of light (93%) and ultrasound (87%), and the PVDF element is a ring structure. It has several advantages: (1) it employs an innovative opto-sono lens structure that can make optical and acoustic foci aligned and effectively improve the signal-to-noise ratio and detection sensitivity; (2) the PVDF element has lower acoustic impedance (2.5 MRayl) that matches well with the human skin tissue, and has the advantages of wide band and high

sensitivity for PA imaging [18]; (3) the waterless coupling mode can provide a rotational angle to accommodate different detected positions when the opto-sono probe is assembled on a universal ball, which is conveniently coupled with the narrow area of the skin surface. Then this new opto-sono probe is used to build a PA dermoscopic system and evaluate its performance with phantom and in human skin experiments.

The schematic of the PA dermoscope is shown in Fig. 1(a). A miniature laser (Model DTL-314QT, pulsed Q -switched Laser, Russia), which operates at a wavelength of 532 nm with a pulse width of 4 ns, is used as the excitation light source and then focused by a convex lens, which passes through a 20 μm pinhole for spatial filtering and, finally, focuses into a single-mode fiber using a plan objective lens (NA 0.1; working distance (WD) 37.5 mm). Figure 1(b) is a photograph of the opto-sono probe with a single-mode fiber shown by the blue dashed rectangle in Fig. 1(a), which consists of a fixed focus collimation (F240FC-532, Thorlabs), an adjustable objective lens (NA 0.1; WD 17 mm; adjust distance 5 mm), and an opto-sono 25 MHz ultrasonic detector [Fig. 1(d)]. A schematic of the PA dermoscope system is shown by the red dashed rectangle in Fig. 1(a). The cross-sectional structure of the detector is shown in Fig. 1(c), which is mainly composed of an opto-sono PS lens (the acoustic impedance of that is about 2.42 MRayl) and a hollow bowl PVDF element. The thickness of the PVDF element is 25 μm , and the diameter of the working PVDF element is 6 mm, with a 1.5 mm center hole for the exit of the laser beam. The PVDF element is coated with silver electrodes at both sides, and then attached to the spherical surface of the PS lens with epoxy resin (301-2, EPO-TEK). The outer

diameter of the detector housing is 15 mm, and the inner conductor of the coaxial cable was bound to the back electrode of the PVDF element with silver epoxy for signaling; a braided shield was bonded to the detector housing for ground. Figure 1(e) shows the optical beam intensity profile at the focal distance, and the laser beam diameter is about 4.3 μm . The opto-sono detector matches with the adjustable objective lens and, finally, realizes the coaxial confocal configuration of the PA dermoscopic system. The opto-sono probe was actuated automatically by a two-dimensional scanner (SmartAct; SCL-2445). The detected PA signals are sequentially amplified with a 50 dB low noise amplifier (LNA-650, RFBAY) digitized with a data acquisition (DAQ) card (M3i.4110, SPECTRUM, 100 MHz sampling frequency), and stored in the computer's hard drive for later data processing. To conform to the American National Standards Institute safety limit (20 mJ/cm^2) [19], we limit the laser pulse energy on the tissue surface to 80 nJ. A LabVIEW program controlled the DAQ process, and the entire system is synchronized with the trigger provided by the scanner-control PC system.

For the PA dermoscope, the field characteristic of the opto-sono detector is a key factor that decides the accuracy of the image reconstruction. To test the acoustic characteristics of the built detector [Fig. 2(a)], the detector was driven by a pulser/receiver (5073PR, Olympus) to emit ultrasound pulses. A hydrophone (HPM02, Precision Acoustics Ltd.) was employed to scan laterally and axially while detecting the ultrasound pulses from the detector [Fig. 2(b)]. The

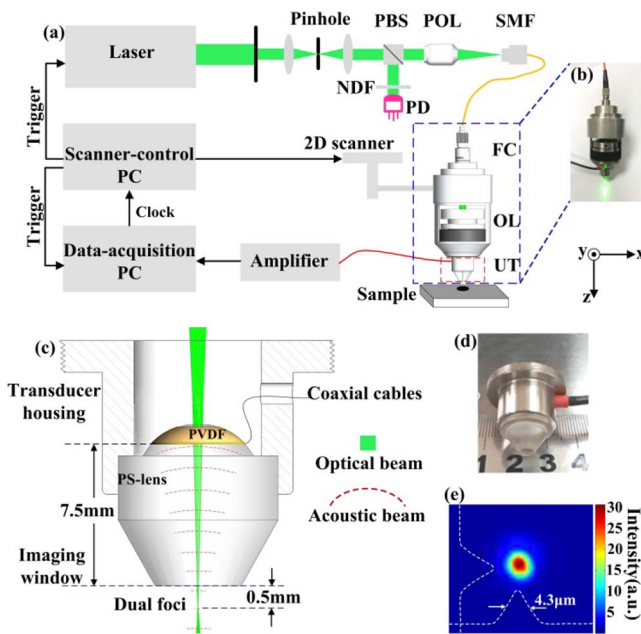


Fig. 1. Schematic of the PA dermoscope system. (a) Schematic of the entire setup. NDF, neutral density filter; PBS, polarizing beam splitter; PD, photodiode; POL, plan objective lens; SMF, single-mode fiber; FC, fiber collimator; AO, adjustable objective; OD, opto-sono detector. (b) Photograph of the opto-sono probe with a single-mode fiber. (c) Cross-sectional structure of the opto-sono detector. (d) Photo image of the opto-sono detector. (e) Optical beam intensity profile at the focal distance.

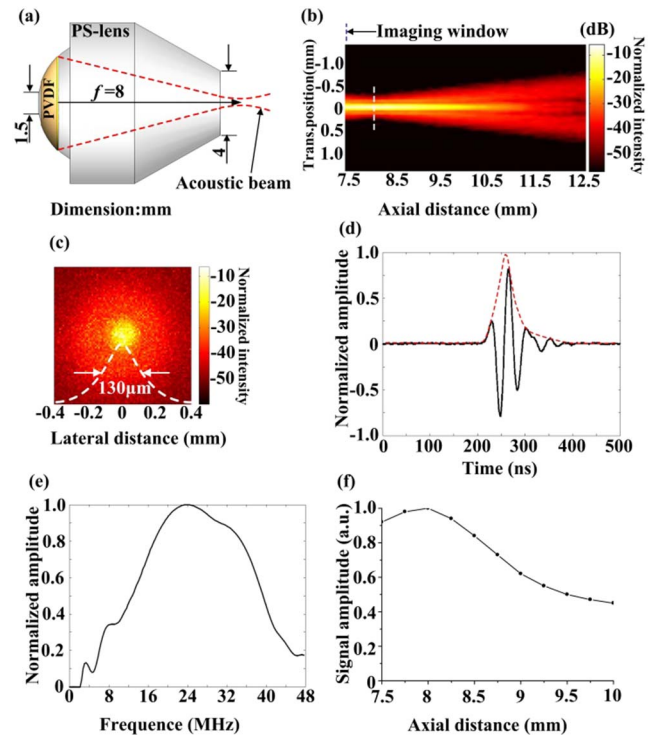


Fig. 2. Acoustic characteristics of the opto-sono detector. (a) Geometry of the detector (side view). (b) Acoustic pressure distribution of the detector. (c) Acoustic beam intensity profile at the focal distance. (d) Pulse response of the detector at the focus. (e) Amplitude-frequency response of the detector. (f) Signal amplitude variation graph.

acoustic beam intensity profile at the focal distance is shown in Fig. 2(c). It is seen that the acoustic field is well focused; the focal length is around 8 mm, and the diameter is about 130 μm at the focal distance. Figure 2(d) shows the pulse response of the detector at the focus (black line), and the red dotted line is the corresponding Hilbert-transformed envelope. The axial resolution can be taken as the full width at half-maximum (FWHM) of the envelope, which is measured to be about 50 μm . The amplitude-frequency response of the detector is shown in Fig. 2(e). Based on the amplitude-frequency response, it determines the central frequency of the detector is about 25 MHz and the fractional bandwidth ($\sim 85\%$) of the detector. Then the focal distance of the detector was experimentally determined by measuring the pulse-echo signals reflected from a quartz block. As shown in the signal amplitude variation graph [Fig. 2(f)], a peak response at a distance of ~ 8 mm from the detector was observed, which is close to the calculated theoretical value.

Lateral and axial resolution experiments were performed to verify the imaging capability of the PA dermoscopic system. A surgical blade was obliquely inserted into the sink shown in Fig. 3(a), and experimentally quantified by imaging the sharp-edged surgical blade indicated in Fig. 3(b), with a scanning step of ~ 2 μm . The fitted edge-spread function (ESF) was estimated from the blade PA data along the white dashed line at the focal distance. The line-spread function (LSF) was calculated as the derivative of the ESF. The FWHM of the LSF defining the highest lateral resolution was estimated to be 4.8 μm , which was slightly larger than the theoretical value (2.7 μm), as shown in Fig. 3(c). Figure 3(d) shows the lateral resolutions of a PA dermoscope as functions of the imaging depth. Due to the deviation from the optical focus position, the optical focusing degrades with depth, deteriorating the lateral resolution of the PA dermoscope. In order to measure

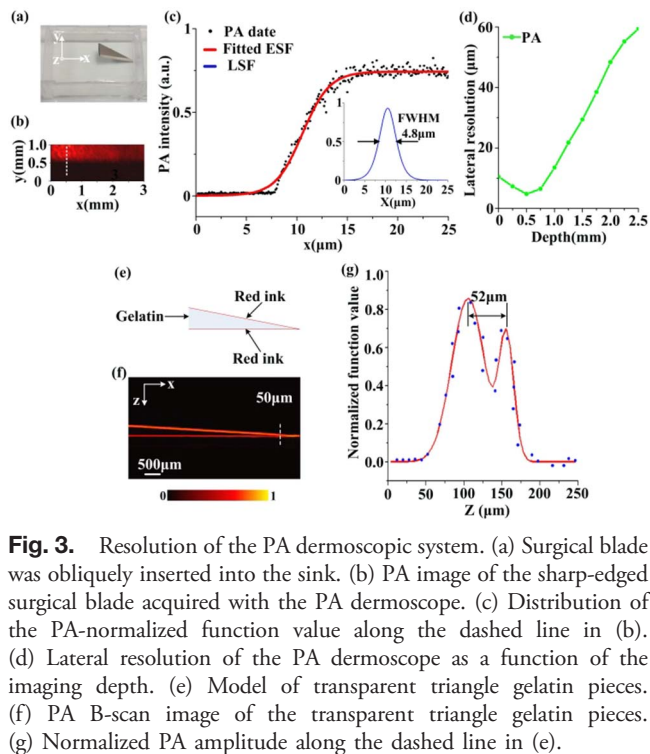


Fig. 3. Resolution of the PA dermoscopic system. (a) Surgical blade was obliquely inserted into the sink. (b) PA image of the sharp-edged surgical blade acquired with the PA dermoscope. (c) Distribution of the PA-normalized function value along the dashed line in (b). (d) Lateral resolution of the PA dermoscope as a function of the imaging depth. (e) Model of transparent triangle gelatin pieces. (f) PA B-scan image of the transparent triangle gelatin pieces. (g) Normalized PA amplitude along the dashed line in (e).

the actual axial resolution, a transparent triangle gelatin pieces was prepared, and two surfaces were coated with red ink as in Fig. 3(e); the transparent triangle gelatin piece was made up of silicone. (The acoustic impedance is about 1.5 MRayl, and the transmission efficiency of light is not less than 90%.) The PA image of the triangle gelatin pieces was shown in Fig. 3(f). Figure 3(g) was the reconstructed profile of the sample marked by the white dotted line in Fig. 3(f). The axial resolution of the profile was estimated to be 52 μm , which matched well with the axial resolution of the built detector in Fig. 2(d).

To demonstrate the capability of the PA dermoscopic system, the structure of the human hand skin was investigated, as shown in Figs. 4(a) and 4(b). The imaging speed of the photoacoustic confocal dermoscope is about 0.25 s per frame, and the maximum depth imaging for the human skin is about 2 mm. All the human experiments followed a protocol approved by the Institutional Review Board administered by the Human Research Protection Office at South China Normal University in Guangzhou. The human skin consists of epidermis, dermis, and subcutaneous tissue, the epidermis includes the stratum corneum (SC) and melanin (M) layers, and there are a lot of blood vessels in the dermis. Hence, it is presumed that the PA map reveals the epidermal structure with SC and M layers and blood vessels in the dermis due to the different optical-absorption characteristics of those layers. Figures 4(f)–4(h) show corresponding consecutive cross-sectional PA maps along white dashed lines in Figs. 4(c)–4(e), respectively. As can be seen, the cross-sectional of the blood vessels is presented in its entirety, and the M layer of the opisthenar is much thicker than that of the palm. The SC and M layers will overlap because of the thick M layers. In addition, the thickness is estimated by the distance between the two yellow dotted lines, and it is seen that the epidermal thickness of the palm is slightly thinner than that of the opisthenar. The results demonstrate that the PA dermoscope is able to reveal the epidermal structure and blood vessels of the dermis.

To further demonstrate the potential clinical applications of the PA dermoscope, the SC and M layers in the human skin were investigated. Figures 5(a) and 5(b) show corresponding consecutive cross-sectional PA images of the adult (c) facial skin and the child (d) facial skin from two volunteers in Figs. 5(c) and 5(d), respectively. A flagrant contrast, the PA imaging of the adult (c) facial skin reveals a significantly thick layer of the SC, and the intensity of the SC of the adult (c) facial skin to that of the child (d) facial skin is about 2.5 times, as shown in Fig. 5(e). Meanwhile, a controlled trial of the M layers was implemented from the consecutive cross-sectional PA images

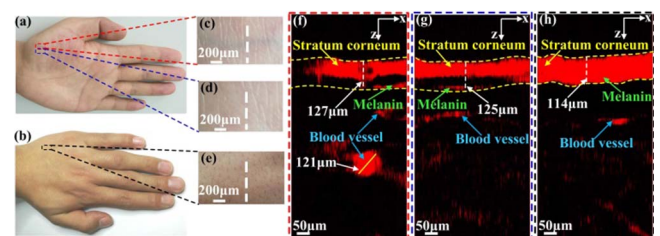


Fig. 4. Photoacoustic mapping of the epidermal structure and blood vessels in the dermis. (a) and (b) Photographs of the human palm and opisthenar. (c)–(e) Detection areas of the human palm and opisthenar. (f)–(h) Consecutive cross-sectional PA maps of the detection areas.

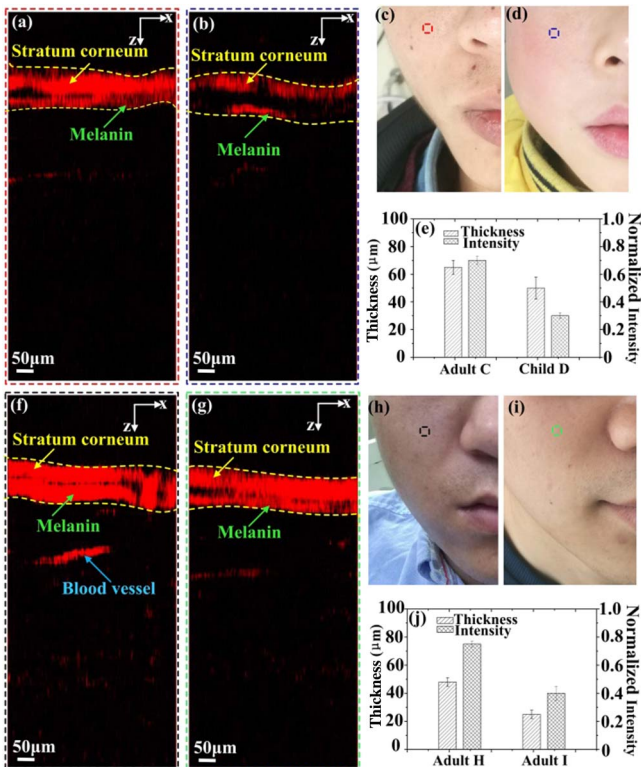


Fig. 5. Measuring and quantifying the SC and M layers by photoacoustic imaging. (a) and (b) Consecutive cross-sectional PA images of (c) the adult and (d) the child facial skin. (c) and (d) Detection areas of the (c) adult and (d) child (d). (e) Statistics, i.e., thickness and intensity of the M layer and the SC from the PA images of the detection areas of (c) the adult and (d) the child. (f) and (g) Consecutive cross-sectional PA images of (h) an adult and (i) the other adult. (h) and (i) Detection areas of (h) the adult and (i) the other adult. (j) Statistics, i.e., thickness and intensity of the M layer and the SC, from the PA maps of the detection areas of (h) the adult and (i) the other adult. (e) and (j) Data were analyzed using Image J software. The personal information for the four volunteers is as follows: (1) age: the ages of volunteers (c), (d), (h), and (i) are 28, 6, 26, and 24, respectively. (2) Gender: the volunteers are all male. (3) Skin color: the skin color of volunteers (c), (d), and (i) is slightly white, and the skin color of volunteer (h) is slightly dark.

of an adult (h) with slightly dark skin [Fig. 5(h)] and the other adult (i) with slightly white skin [Fig. 5(i)], as shown in Figs. 5(f) and 5(g). As it turns out, PA imaging of the adult (h) with slightly dark skin reveals a significantly thick layer of M layers, and the intensity of the SC of the adult (h) facial skin to that of the adult (i) facial skin is about doubled, as shown in Fig. 5(j).

These results demonstrate that the PA dermoscope can clearly reveal the epidermal structure. Therefore, by quantifying the intensity and measuring the thickness of the SC and M layers, the PA dermoscope can provide spatial characterization and quantitative parameters (the SC and M layer thickness, pigment concentration) for analyzing keratinization skin disease and pigmented skin lesions.

In conclusion, a waterless coupling and impedance matching opto-sono probe was designed for the PA dermoscope. We

have demonstrated that the built probe can make a PA dermoscopic system achieve quantification and depth-imaging capability, and be able to create volumetric vascular images with high contrast and high resolution that are label free. In addition, the PA dermoscope equipped with the opto-sono probe may have a useful role in imaging the abnormal pigment (Cafe-au-lait, Freckle, and Chloasma) located in the epidermis and the abnormal plexus (nevus flammeus, capillary hemangioma) located in the dermis, providing an ability to not only measure the SC, M layers, and blood vessels, but also to quantify the amount of them. This Letter is promising for making clear the distribution of pigments of the skin and the changes for chroma values of pigment-diseased skin diseases during laser treatments. In addition, it might support a cure standard of clinical laser therapy quantitatively.

Funding. National High Technology Research and Development Program of China (2015AA020901); National Natural Science Foundation of China (NSFC) (61331001, 61627827, 81630046, 91539127); Science and Technology Planning Project of Guangdong Province, China (2014A020215031, 2014B020215003, 2015B020233016); Distinguished Young Teacher Project in Higher Education of Guangdong, China (YQ2015049); Science and Technology Youth Talent for Special Project of Guangdong, China (2015TQ01X882).

REFERENCES

- L. V. Wang and S. Hu, *Science* **335**, 1458 (2012).
- S. Hu, P. Yan, K. Maslov, J. M. Lee, and L. V. Wang, *Opt. Lett.* **34**, 3899 (2009).
- S. A. Sharif, E. Taydas, A. Mazhar, R. Rahimian, K. M. Kelly, B. Choi, and A. J. Durkin, *Br. J. Dermatol.* **167**, 1215 (2013).
- D. Jasaitiene, S. Valiukeviciene, G. Linkeviciute, R. Raisutis, E. Jasiuniene, and R. Kazys, *J. Eur. Acad. Dermatol. Venereol.* **25**, 375 (2011).
- D. Xu, S. Yang, Y. Wang, Y. Gu, and D. Xing, *Biomed. Opt. Express* **7**, 2095 (2016).
- K. Peng, L. He, B. Wang, and J. Xiao, *Biomed. Opt. Express* **6**, 135 (2015).
- M. Jeon, J. Kim, and C. Kim, *Med. Biol. Eng. Comput.* **54**, 283 (2016).
- Y. Liu, X. Yang, D. Zhu, R. Shi, and Q. Luo, *Opt. Lett.* **38**, 4236 (2013).
- Z. Xie, S. Jiao, H. F. Zhang, and C. A. Puliafito, *Opt. Lett.* **34**, 1771 (2009).
- L. Xi, C. Song, and H. Jiang, *Opt. Lett.* **39**, 3328 (2014).
- Y. Wang, D. Xu, S. Yang, and D. Xing, *Biomed. Opt. Express* **7**, 279 (2016).
- J. R. Rajian, P. L. Carson, and X. Wang, *Opt. Express* **17**, 4879 (2009).
- P. Subochev, *Opt. Lett.* **41**, 1006 (2016).
- Z. J. Chen, S. H. Yang, and D. Xing, *Opt. Lett.* **37**, 3414 (2012).
- L. Li, C. Yeh, S. Hu, L. Wang, B. T. Soetikno, R. Chen, Q. Zhou, K. K. Shung, K. I. Maslov, and L. V. Wang, *Opt. Lett.* **39**, 2117 (2014).
- Q. Zhou, K. H. Lam, H. Zheng, W. Qiu, and K. K. Shung, *Prog. Mater. Sci.* **66**, 87 (2014).
- K. S. Ramadan, D. Sameoto, and S. Evoy, *Smart Mater. Struct.* **23**, 033001 (2014).
- G. H. Feng and G. Y. Chu, *Sens. Actuators A* **208**, 130 (2014).
- Laser Institute of America, American National Standard for Safe Use of Lasers," ANSI Z136.1-2007 (American National Standards Institute, 2007).